

# Gradient-trained Weights in Wide Neural Networks Align Layerwise to Error-scaled Input Correlations

Akhilan Boopathy

Massachusetts Institute of Technology  
akhilan@mit.edu

Ila Fiete

Massachusetts Institute of Technology  
fiete@mit.edu

## Abstract

Recent works have examined how deep neural networks, which can solve a variety of difficult problems, incorporate the statistics of training data to achieve their success. However, existing results have been established only in limited settings. In this work, we derive the layerwise weight dynamics of infinite-width neural networks with nonlinear activations trained by gradient descent. We show theoretically that weight updates are aligned with input correlations from intermediate layers weighted by error, and demonstrate empirically that the result also holds in finite-width wide networks. The alignment result allows us to formulate backpropagation-free learning rules, named Align-zero and Align-ada, that theoretically achieve the same alignment as backpropagation. Finally, we test these learning rules on benchmark problems in feedforward and recurrent neural networks and demonstrate, in wide networks, comparable performance to backpropagation.

## 1 Introduction

Deep neural networks trained with gradient descent are surprisingly successful in solving a variety of tasks and exhibit a moderate degree of generalization [1] and transferability [2]. However, it has remained theoretically difficult to understand what aspects of the training data the networks use – and how – to achieve their success. One approach is to examine the internal representations of deep neural networks by focusing on learned features, the topic of several recent works [3, 4, 5, 6, 7, 8].

In this work, we focus on investigating neural network representations through the perspective of *alignment* between the weights of a neural network and statistics of input data. Prior work has shown that in deep linear networks, intermediate layer weights have singular values and singular vectors related to the correlation matrix between the inputs and training labels, revealing that deep linear networks encode hierarchical structures in their inputs [8]. [7] investigate the representations of nonlinear neural networks trained with randomized labels and show theoretically that the first layer of such a network has weights with singular vectors in the same directions as the eigenvectors of the input covariance matrix: the weights are aligned with the inputs. The authors also empirically demonstrate partial alignment in later layers. Although the previous alignment effects were only proved theoretically in the specialized settings of deep linear networks and early layers of networks trained with random labels, the findings suggest a deeper underlying alignment effect in standard neural networks trained with gradient descent.

We extend analyses on how data shapes network weights to all layers in nonlinear deep networks, by considering alignment in *wide* neural networks. Specifically, we leverage Neural Tangent Kernel (NTK) theory [9], which allows for analysis of neural networks under a particular limit of infinite-width, which we will refer to as the NTK limit. Using NTK theory, we show for infinitely-wide networks in the NTK limit an alignment effect between intermediate layer weights and statistics of corresponding layers’ activations. Our analysis indicates that even though neural network functions and training dynamics are complex and nonlinear, under an NTK limit-inducing training regime,

intermediate layer weights of neural networks trained with gradient descent collect simple layerwise statistics of input data. The locality of the weights’ dependence on the data propagated through the network prompts us to consider whether wide neural networks can be trained with simplified learning rules that reproduce the alignment effect without using backpropagation, the most common implementation of gradient descent in neural networks. This direction also has relevance in finding biologically-plausible learning rules for neural networks that avoid the biological difficulties in implementing backpropagation [10, 11, 12, 13, 14, 15, 16, 17, 18]. Such learning rules may yield better understanding of the learning mechanisms in the brain, and may help further unify artificial neural networks with their biological counterparts.

In this paper, we make the following specific contributions:

- By analyzing the parameter dynamics of neural networks in the NTK limit, we show theoretically that gradient descent on infinite-width neural networks produces weights that are aligned with network layers in the following sense: the correlation matrix of the weight change at a particular layer is equal to an *error-weighted* correlation matrix of the layer values at the same layer.
- We propose an *alignment score* to measure the extent of this alignment in finite-width networks and empirically demonstrate input-weight alignment in wide, finite-width neural networks trained in the NTK regime.
- We develop two backpropagation-free learning rules, called *Align-zero* and *Align-ada*, that are designed to reproduce the input-weight alignment effect. We prove the equivalence between these learning rules and gradient descent in the infinite-width limit. Moreover, we empirically show that the learning rules achieve comparable performance to gradient descent on wide convolutional neural networks (CNNs) and wide recurrent neural networks (RNNs) in the NTK training regime. In this regime, the proposed learning rules outperform other backprop-free baseline learning rules including feedback alignment (FA) [13] and direct feedback alignment (DFA) [14].

## 2 Related Work

**Wide neural networks.** Recently, randomly initialized infinite-width deep neural networks have been shown to be equivalent to Gaussian processes [19, 20]. Moreover, gradient descent on infinite-width networks can be viewed as a kernel method: gradient descent on infinite width networks is equivalent to kernel regression under the Neural Tangent Kernel (NTK) [9]. This insight has been used to train neural networks exactly in the infinite limit [21]. NTK theory has also been used to show theoretically and empirically that wide *finite-width* neural networks evolve as *linearized* models in terms of their parameters [22]. [23] further shows that the correspondence between finite-width wide networks and infinite width networks is strongest at small learning rates among other results.

We highlight that many results in the above works are only applicable under a specific *neural tangent* parameterization, or equivalently under standard parameterization under a specific choice of width-dependent learning rate [22], which leads to the NTK infinite-width limit. Recent work has shown that there are an infinite number of infinite-width limits, with certain limits, including the NTK limit, exhibiting an equivalence to kernel regression and other limits allowing for *feature learning* in the infinite-limit [24]. In this work we focus on the NTK limit as it is the most studied and has the most analytical tools available. We leave an extension of our results to other infinite-width limits as future work to be explored.

**Biologically-plausible learning.** In an effort to develop accurate models of learning in the brain, researchers have developed a number of biologically-plausible learning algorithms for neural networks. These algorithms avoid some of the biologically implausible aspects of backpropagation, the standard algorithm to train artificial neural networks. These aspects include 1) the fact that forward propagation weights must equal backward propagation weights throughout the training process, known as the weight transport problem [13], 2) the asymmetry of a nonlinear forward propagation computation and a linear backward propagation computation [12] and 3) the alternation of forward and backward passes through the network and the computation of nonlinear activation function derivatives during the backward pass [14].

Feedback alignment (FA) [13] addresses weight transport by showing that backward weights need not equal the corresponding forward weights for effective learning. Direct feedback alignment (DFA) further shows the effectiveness of passing feedback directly to intermediate layers, alleviating the need for a backward pass [14]. Greedy layerwise learning takes a different approach and trains different layers of a neural networks independently, avoiding global feedback altogether [25]. Kernel RNN learning (KeRNL) may be viewed as a generalization of DFA to RNNs with a learned feedback pathway [18]. Unfortunately, while these algorithms perform comparably to backpropagation on small tasks, algorithms that avoid weight transport have difficulties scaling to larger-scale tasks [16]. Following this line of work, in this paper, we propose learning rules that avoid weight transport. However, unlike previous works we prove an equivalence between our learning rules and backpropagation in the limit of infinite-width networks. We believe this provides a strong theoretical reason to expect our learning rules to be as scalable as gradient descent given sufficiently wide networks.

### 3 Alignment Between Layers and Weights

In this section, we introduce the concept of alignment between the layers and weights of a neural network. We then prove that this alignment occurs in infinite-width networks, showing that weights in infinite width networks capture layerwise statistics of input data. Furthermore, we introduce an *alignment score* metric to quantify alignment in finite width networks. Using this metric, we empirically demonstrate alignment between layers and weights in finite-width networks.

#### 3.1 Input-Weight Alignment

We consider an  $N$ -layer neural network  $f(x)$  with input  $x$ . We denote the activation function as  $\sigma$  and weights and biases  $W_l$  and  $b_l$  at layer  $l$ . Throughout this paper, we use the neural tangent parameterization of weights [9]. We denote the pre-activation layer values at layer  $l$  as functions  $z_l(x)$  of input  $x$ . The layer pre-activations are defined as:

$$z_l(x) = \frac{1}{\sqrt{m_{l-1}}} W_l \sigma(z_{l-1}(x)) + b_l \quad (1)$$

for  $l = 1, \dots, N$  where  $f(x) = z_N(x)$  and  $m_{l-1}$  is the dimensionality of  $z_{l-1}(x)$ . For notational convenience we denote  $\sigma(z_0(x)) = x$ . Next, we assume that the network parameters are trained with gradient flow of learning rate  $\eta$  on a supervised learning task with loss function  $\mathbb{E}_{p_x}[L(f(x), y(x))]$  where  $y(x)$  are targets and  $p_x$  denotes the finite-supported training distribution over inputs  $x$ . We denote the parameter values at time  $t$  of training with superscript  $(t)$ : layer  $l$  weights and biases at training time  $t$  are denoted  $W_l^{(t)}$  and  $b_l^{(t)}$ . Similarly, we denote the overall network function and intermediate-layer pre-activations at time  $t$  as  $f^{(t)}(x)$  and  $z_l^{(t)}(x)$  respectively.

To define the concept of alignment, it is convenient to define a layerwise *weight-change correlation matrix*  $\Delta_l^{(t)}$ :

$$\Delta_l^{(t)} = (W_l^{(t)} - W_l^{(0)})^T (W_l^{(t)} - W_l^{(0)}). \quad (2)$$

This matrix represents the correlation between different *columns* of the weight change since initialization,  $W_l^{(t)} - W_l^{(0)}$ . This matrix captures all the information about  $W_l^{(t)} - W_l^{(0)}$  up to rotations of the columns since if  $W_l^{(t)} - W_l^{(0)}$  has singular value decomposition  $USV^T$ , then  $\Delta_l^{(t)} = VS^T SV^T$ . Intuitively, the elements of  $\Delta_l^{(t)}$  represent the similarity between post-activation units of layer  $l - 1$  in terms of how they impact the next layer. If the weight initializations are small ( $\|W_l^{(0)}\| \approx 0$ ), then  $\Delta_l^{(t)}$  is approximately equal to the weight correlation matrix  $W_l^{(t)T} W_l^{(t)}$ . However, we focus on the weight change correlation as it is easier to analyze in the infinite-width limit as we will show.

We also define a layerwise *weighted input activity correlation matrix*  $\Sigma_{l,q}^{(t)}$  as the correlation between post-activations under a particular pairwise weighting of inputs  $q(x_1, x_2)$ :

$$\Sigma_{l,q}^{(t)} = \mathbb{E}_{x_1 \sim p_x, x_2 \sim p_x} [\sigma(z_{l-1}^{(t)}(x_1)) q(x_1, x_2) \sigma(z_{l-1}^{(t)}(x_2))^T] \quad (3)$$

Finally, we say that activities and weights are aligned for a weighting  $q$  when the activity correlation matrix is proportional to the weight correlation matrix:

$$\Sigma_{l,q}^{(t)} = k \Delta_l^{(t)} \quad (4)$$

for some positive constant  $k$ . When the weights are aligned with input activities, the weights can be fully specified as a function of the corresponding layer’s input correlation matrix up to rotation. In other words, alignment implies that weights capture layer-local statistics of the input data.

Note that our notion of alignment is stronger than the one proposed in [7] since we not only require the eigenvectors of the weight change correlation matrix and input activity correlation matrix to be equal, but also require the corresponding eigenvalues to be proportional to each other. We also note the following additional differences with [7]: 1) we use the weight change correlation matrix instead of the weight correlation matrix, 2) we consider the input correlation matrix instead of the input *covariance* matrix which normalizes layer activations to have mean zero, 3) we compute input correlation matrices over a general pairwise weighting  $q(x_1, x_2)$  instead of restricting the weighting to the delta function  $q(x_1, x_2) = \delta(x_1, x_2)$ .

### 3.2 Alignment in infinite-width

In the infinite-width limit, layerwise inputs and weights are aligned under a specific weighting  $q_l^{(t)}(x_1, x_2)$  that depends only on the gradients of the network at initialization and an *integrated-error* function  $\delta^{(t)}(x) \in \mathbb{R}^{m_N}$ :

$$\delta^{(t)}(x) = \eta \int_0^t \nabla_{z_N} L(f^{(\tau)}(x), y(x)) d\tau \quad (5)$$

This quantity captures the averaged influence  $x$  has on the function  $f(x)$  over the course of training. Note that this quantity only depends on the output values of the network and effectively measures the average error incurred by the network outputs on point  $x$  across the course of training. We also define a layerwise kernel  $\Gamma_l(x_1, x_2) \in \mathbb{R}^{m_N \times m_N}$  as:

$$\Gamma_l(x_1, x_2) = \nabla_{z_l} f^{(0)}(x_1)^T \nabla_{z_l} f^{(0)}(x_2) \quad (6)$$

This quantifies the similarity in the gradients of  $x_1$  and  $x_2$  at layer  $l$ . It depends only on the initial configuration of the network. Finally, we define  $q_l^{(t)}(x_1, x_2) \in \mathbb{R}$  as:

$$q_l^{(t)}(x_1, x_2) = \delta^{(t)}(x_1)^T \Gamma_l(x_1, x_2) \delta^{(t)}(x_2) \quad (7)$$

Intuitively, pairs of points which influence the network  $f(x)$  similarly will be weighted positively and points which have opposite influences on the network will be weighted negatively. Note that this weighting produces an input activity correlation  $\Sigma_{l, q_l^{(t)}}^{(t)}$  whose only dependence on the targets  $y(x)$  is through the integrated-error  $\delta^{(t)}(x)$ . Therefore,  $\Sigma_{l, q_l^{(t)}}^{(t)}$  is an *error-weighted* correlation matrix of the data. We can then show alignment between input activations and weights in the infinite-width limit:

**Proposition 1.** *Assume layers are randomly initialized according to the neural tangent initialization [9]. Also, assume that the nonlinearity  $\sigma(\cdot)$  has bounded first and second derivatives. Suppose the network is trained with continuous gradient flow with learning rate  $\eta$  on the mean-squared error loss for  $T$  time such that  $\max_x \|y(x) - f^{(t)}(x)\|_2$  is uniformly bounded in  $t \in [0, T]$ . Then, in the sequential limit  $\lim_{m_N \rightarrow \infty} \lim_{m_{N-2} \rightarrow \infty} \dots \lim_{m_1 \rightarrow \infty}$ :*

$$\frac{1}{\sqrt{m_{l-1}}} \left\| \frac{1}{m_{l-1}} \Sigma_{l, q_l^{(t)}}^{(0)} - \Delta_l^{(t)} \right\|_{op} = 0 \quad (8)$$

*Proof.* See Appendix A for a proof. □

Proposition 1 equates the layerwise input correlation at time 0 with  $m_{l-1} \Delta_l^{(t)}$ . Conceptually, as layer widths increase, the feedback Jacobian  $\nabla_{z_l} f^{(t)}(x)$  and intermediate-layer activations change vanishingly little over the course of training, making the weight correlation proportional to the input correlation. The interpretation of the result hinges on the nature of the pairwise weighting  $q_l^{(t)}(x_1, x_2)$ . As discussed,  $q_l^{(t)}(x_1, x_2)$  intuitively captures the similarity in the errors from  $x_1$  and  $x_2$ . Thus, Proposition 1 can be interpreted as saying that the weight changes of an infinite-width neural network reflect error-weighted correlation statistics of the inputs from corresponding intermediate layers.

### 3.3 Alignment in finite-width

Although Proposition 1 applies to infinite-width networks, we show that alignment approximately holds in finite-width networks of sufficient width. In finite-width networks, we can empirically quantify the degree of alignment through an *alignment score* that measures the similarity between the weight correlation  $\Delta_l^{(t)}$  and the time 0 input correlation  $\Sigma_{l,q_l^{(t)}}^{(0)}$ . First, observe that the correlation matrices are both symmetric matrices of the same dimension. Recall that the set of all symmetric matrices of a certain dimension forms a vector space. Therefore, it is natural to use the cosine of the angle between the two matrices as an alignment score  $S$ :

$$S = \text{tr}(\Delta_l^{(t)} \Sigma_{l,q_l^{(t)}}^{(0)}) \text{tr}(\Delta_l^{(t)})^{-1/2} \text{tr}(\Sigma_{l,q_l^{(t)}}^{(0)})^{-1/2} \quad (9)$$

This score is in the range  $[-1, 1]$  with 1 indicating perfect alignment. For wide neural networks, it may not be computationally efficient to operate directly on  $\Delta_l^{(t)}$  and  $\Sigma_{l,q_l^{(t)}}^{(0)}$  because their sizes scale quadratically with layer width. Instead, the score can be computed in terms of  $\Delta_l^{(t)} z$  and  $\Sigma_{l,q_l^{(t)}}^{(0)} z$  when  $z$  is sampled from a unit Gaussian  $N(0, I)$ :

$$S = \mathbb{E}_z [z^T \Delta_l^{(t)} \Sigma_{l,q_l^{(t)}}^{(0)} z] \left( \mathbb{E}_z [\|\Delta_l^{(t)} z\|_2^2] \mathbb{E}_z [\|\Sigma_{l,q_l^{(t)}}^{(0)} z\|_2^2] \right)^{-1/2} \quad (10)$$

$\Delta_l^{(t)} z$  and  $\Sigma_{l,q_l^{(t)}}^{(0)} z$  are computed as a series of matrix-vector products:

$$\Delta_l^{(t)} z = (W_l^{(t)} - W_l^{(0)})^T (W_l^{(t)} - W_l^{(0)}) z \quad (11)$$

$$\Sigma_{l,q_l^{(t)}}^{(0)} z = m_{l-1} (W_l^{*(t)} - W_l^{(0)})^T (W_l^{*(t)} - W_l^{(0)}) z \quad (12)$$

where  $W_l^{*(t)}$  is defined as:

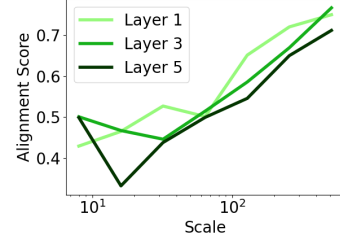
$$W_l^{*(t)} = W_l^{(0)} + \frac{\eta}{\sqrt{m_{l-1}}} \mathbb{E}_{p_x} [\nabla_{z_l} f^{(0)}(x) \left[ \int_0^t \nabla_{z_N} L(f^{(t)}(x), y(x)) d\tau \right] \sigma(z_{l-1}^{(0)}(x))^T] \quad (13)$$

We have set  $W_l^{*(0)} = W_l^{(0)}$ . Note that  $W_l^{*(0)}$  can be obtained by starting at the initial condition  $W_l^{*(0)} = W_l^{(0)}$  and applying the following dynamics:

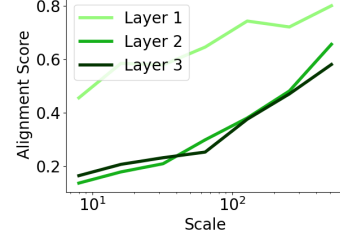
$$\dot{W}_l^{*(t)} = \frac{\eta}{\sqrt{m_{l-1}}} \mathbb{E}_{p_x} [\nabla_{z_l} f^{(0)}(x) \nabla_{z_N} L(f^{(t)}(x), y(x)) \sigma(z_{l-1}^{(0)}(x))^T]. \quad (14)$$

Then,  $W_l^{*(t)}$  is computed by simply training a network with the above learning rule. This alignment computation naturally yields an interpretation of the alignment score as a similarity between the parameters of a network and the corresponding network trained with initialized activations  $\sigma(z_{l-1}^{(0)}(x))$  and initialized feedback Jacobian  $\nabla_{z_l} f^{(0)}(x)$ . We further investigate variants of the learning rule of Equation (14) in Section 4.

Next, we use the alignment scores to evaluate alignment in finite-width networks trained on CIFAR-10 [26] and KMNIST [27], as a function of network width. We train an 8 (CIFAR-10) or 4 (KMNIST) layer CNN on the mean squared error loss and vary the number of convolutional filters in the intermediate layers from 8 to 512. See Section 5 for further architectural and hyperparameter details. In Figure 1, we find that alignment scores increase with network width, consistent with our prediction of perfect alignment in infinite width. Generally, alignments are lower in later layers of network, suggesting the infinite-width correspondence holds best in early layers. Nevertheless, the results illustrate that in sufficiently wide finite-width networks, intermediate layer weights indeed capture



(a) CIFAR-10



(b) KMNIST

Figure 1: Alignment scores at different layers of convolutional neural networks with different layer widths trained on the CIFAR-10 (8 layers) and KMNIST (4 layers). The scale of the architecture is denoted  $\times n$ , where  $n$  is the number of filters in intermediate layers.

local statistics of the corresponding layers' inputs. See Appendix Tables 1, 2 for full tabulated results. In Appendix Figure 7, we plot the evolution of alignment scores during training and find that they are initially high and slowly decrease during training as parameters drift from initialization. We also plot baseline alignment scores in networks with randomly permuted weights after training and find low alignment, validating the statistical significance of our alignment scores.

## 4 Simplified Training Rules Produce Alignment

Prompted by the observation that wide finite-width networks exhibit high input-weight alignment, we consider whether simplified learning rules that produce alignment also yield well-performing networks. Specifically, we consider two variants of the learning rule used to compute alignment scores in the previous section. We show theoretically that the learning rules are equivalent to gradient descent in the infinite width limit. In Section 5, we perform extensive experiments assessing the performance of these learning rules in finite-width networks.

Before considering simplified training rules, we examine the learning rule of gradient descent:

$$\begin{aligned}\dot{W}_l^{(t)} &= \frac{\eta}{\sqrt{m_{l-1}}} \mathbb{E}_{p_x} [\nabla_{z_l} f^{(t)}(x) \nabla_{z_N} L(f^{(t)}(x), y(x)) \sigma(z_{l-1}^{(t)}(x))^T d\tau] \\ \dot{b}_l^{(t)} &= \eta \mathbb{E}_{p_x} [\nabla_{z_l} f^{(t)}(x) \nabla_{z_N} L(f^{(t)}(x), y(x)) d\tau] \quad (15)\end{aligned}$$

In the infinite-width limit, we expect  $\nabla_{z_l} f^{(t)}(x)$  and  $\sigma(z_{l-1}^{(t)}(x))$  to remain unchanged over the course of training, which enables input-weight alignment. The simplified learning rules are found by setting both of these quantities to their values at initialization. Specifically, we find the *Align-zero* learning rule by setting both quantities to their initialization values at time 0:

$$\begin{aligned}\dot{W}_{l,al.0}^{(t)} &= \frac{\eta}{\sqrt{m_{l-1}}} \mathbb{E}_{p_x} [\nabla_{z_l} f^{(0)}(x) \nabla_{z_N} L(f_{al.0}^{(t)}(x), y(x)) \sigma(z_{l-1}^{(0)}(x))^T] \\ \dot{b}_{l,al.0}^{(t)} &= \eta \mathbb{E}_{p_x} [\nabla_{z_l} f^{(0)}(x) \nabla_{z_N} L(f_{al.0}^{(t)}(x), y(x))] \quad (16)\end{aligned}$$

where  $f_{al.0}^{(t)}$  represents the network with parameter values  $W_{l,al.0}^{(t)}$ . The difference between the rule of Equation (16) and the earlier alignment computation rule of Equation (14) is that the previous rule uses output gradients  $\nabla_{z_N} L(f^{(t)}(x), y(x))$  of the original network  $f(x)$  trained with gradient descent, while the above rule uses output gradients  $\nabla_{z_N} L(f_{al.0}^{(t)}(x), y(x))$  of the network  $f_{al.0}(x)$  trained with the above learning rule. Unlike the earlier rule, the above learning rule does not require an additional network  $f(x)$  trained with gradient descent; it can be used by itself to compute  $f_{al.0}^{(t)}(x)$ .

**Remark on difference with [22]** Note that our Align-zero learning rule differs subtly but importantly from the linearized networks of [22]. Both formulations use the learning dynamics of Equation (14) for their parameters – which is linear in the parameters. However, the two formulations apply Equation (14) as a function of their respective activation dynamics  $f_{al.0}^{(t)}(x), f_{lin}^{(t)}(x)$ . While our activation dynamics  $f_{al.0}^{(t)}(x)$  are a nonlinear neural network with parameters  $W_{l,al.0}^{(t)}$  and  $b_{l,al.0}^{(t)}$ , the activation dynamics  $f_{lin}^{(t)}(x)$  of [22] are themselves linear and *not a neural network*. Rather,  $f_{lin}^{(t)}(x)$  is the first order term in the Taylor expansion of the neural network  $f_{al.0}^{(t)}(x)$ :

$$\begin{aligned}f_{al.0}^{(t)}(x) &= f^{(0)}(x) + \nabla_{\theta} f^{(0)}(x)^T (\theta^{(t)} - \theta^{(0)}) + O((\theta^{(t)} - \theta^{(0)})^2) \\ &= f_{lin}^{(t)}(x) + O((\theta^{(t)} - \theta^{(0)})^2) \quad (17)\end{aligned}$$

where  $\theta^{(t)}$  represents the parameters of both functions. While the two types of linearization behave similarly near initialization, our approach linearizes only the parameter dynamics, while the approach of [22] also linearizes the network's activation dynamics. We focus on only linearizing the parameter dynamics because our goal is to study learning rules for actual (non-linearized) neural networks.

In recognition of the possibility that network activations might change slightly in wide but finite-width networks, we may alter the Align-zero rule to allow parameter learning to *adapt* to the locally

available values  $\sigma(z_{l-1}^{(t)}(x))$ , instead of fixing them to their values at initialization. This results in the *Align-ada* learning rule:

$$\dot{W}_{l,al-ada}^{(t)} = \frac{\eta}{\sqrt{m_{l-1}}} \times \mathbb{E}_{p_x} [\nabla_{z_l} f^{(0)}(x) \nabla_{z_N} L(f_{al-ada}^{(t)}(x), y(x)) \sigma(z_{l-1}^{(t)}(x))^T] \\ \dot{b}_{l,slin}^{(t)} = \eta \mathbb{E}_{p_x} [\nabla_{z_l} f^{(0)}(x) \nabla_{z_N} L(f_{al-ada}^{(t)}(x), y(x))] \quad (18)$$

where  $f_{al-ada}(x)$  denotes the network with parameters  $W_{l,al-ada}^{(t)}, b_{l,al-ada}^{(t)}$  trained by Align-ada. See Appendix C, Algorithms 1 and 2, for pseudocode and full procedures for training with Align-zero and Align-ada. Also see Figure 2 for a visual comparison of Align-zero and Align-ada.

Both Align-zero and Align-ada avoid continual weight transport as they replace the backpropagation Jacobian  $\nabla_{z_l} f^{(t)}(x)$  with a fixed feedback Jacobian  $\nabla_{z_l} f^{(0)}(x)$ . However, the rules still require computing the fixed-over-learning feedback function  $\nabla_{z_l} f^{(0)}(x)$ , the backpropagation Jacobian at time 0. This may be difficult to compute biologically; nevertheless, we believe that such a fixed feedback function would be significantly easier to explain biologically compared to backpropagation which requires constant synchronization or mirroring of the forward and feedback weights. Next, we show that Align-ada and Align-zero are *equivalent* to gradient descent in the limit of infinite-width:

**Proposition 2.** *Under the same training conditions in Proposition 1, in the sequential limit  $\lim_{m_{N-1} \rightarrow \infty} \lim_{m_{N-2} \rightarrow \infty} \dots \lim_{m_1 \rightarrow \infty}$ :*

$$f^{(t)}(x) = f_{al-0}^{(t)}(x) = f_{al-ada}^{(t)}(x) \quad (19)$$

*Proof.* See Appendix B for a proof. □

This result establishes that simplified, backprop-free learning rules that are designed to produce input-weight alignment are *as effective as gradient descent in the infinite-width limit*. Indeed, as our proof suggests, a wide variety of learning rules may be equivalent to gradient descent in the infinite-width limit. Moreover, given our observation that wide finite-width networks exhibit high input-weight alignment, Proposition 2 suggests that these learning rules might be effective loss-optimizing rules in finite-width networks. Finally, note that while we use the notation of feedforward networks, our analysis also applies to recurrent neural networks and our learning rules can be adapted to recurrent networks as shown in Appendix D. In the next section, we empirically investigate the effectiveness of the Align-ada and Align-zero learning rules for both feedforward and recurrent networks.

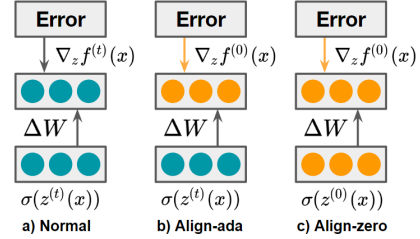


Figure 2: Visual comparison of weight updates  $\Delta W$  in normal training (via gradient descent) and alignment-based training (Align-ada and Align-zero).

## 5 Experiments on Task Performance

In this section, we train finite-width networks using Align-ada and Align-zero and compare their performance to normal training by gradient descent and other backprop-free baseline learning methods. We assess the efficacy of Align-ada and Align-zero across different network widths and learning rates. We conduct experiments on CNNs trained on CIFAR-10 [26], KMNIST [27] and ImageNet [28] and RNNs trained on an addition task. Note that our goal with these experiments is not to optimize performance to beat state-of-the-art results on the tasks but rather to demonstrate both the validity of the theoretical work for finite-width networks and to show in direct comparisons (within the NTK training regime) that Align-zero and Align-ada approach the performance of backpropagation.

### 5.1 Results on CIFAR-10 and KMNIST

**Dataset and baselines** We compare learning methods on CNNs with 7 (CIFAR-10) or 3 (KMNIST) convolutional layers followed by global average pooling and a final fully connected layer. We defer additional architecture and hyperparameter details to Appendix E. We compare the performance of Align-ada and Align-zero against gradient descent (denoted Normal). We also compare with training

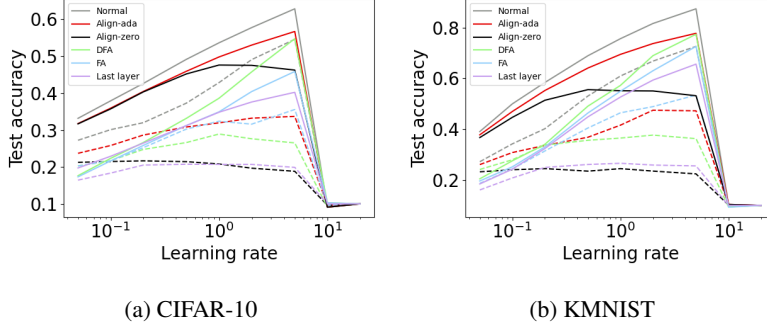


Figure 3: Test set accuracies of different learning rules (Normal, Align-ada, Align-zero, Last layer, DFA, FA) as a function of learning rate on CNNs trained on CIFAR-10 and KMNIST. Solid lines: 256 convolutional filters per layer; dashed: 8 convolutional filters.

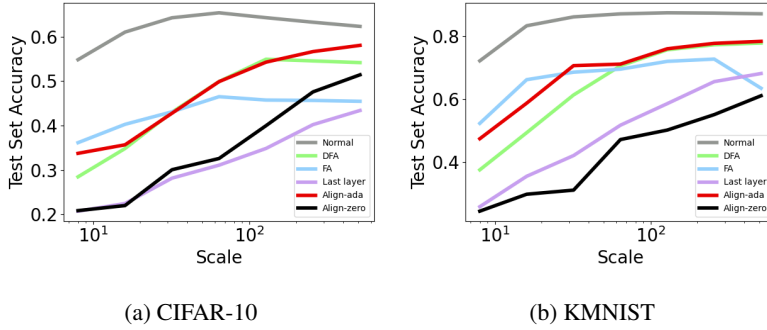


Figure 4: Test set accuracies of different learning rules (Normal, Align-ada, Align-zero, Last layer, DFA, FA) as a function of network scale of CNNs trained on CIFAR-10 and KMNIST.

only the last fully connected layer of the network, leaving intermediate layer parameters fixed, which provides a useful baseline to check that other methods are optimizing intermediate layer parameters (denoted Last layer); with feedback alignment (denoted FA) [13] which uses fixed random feedback weights; and with direct feedback alignment (denoted DFA) [25], which replaces the  $x$ -dependent feedback Jacobian  $\nabla_{z_l} f^{(0)}(x)$  of Align-zero with a constant random matrix.

**Varying learning rate** In Figure 3, we plot the performance of Align methods vs. baselines over a grid search of learning rates in  $[0.05, 20]$  for a narrow and wide network. As illustrated, at small learning rates the performance of Align-ada, Align-zero and Normal is very close on both CIFAR-10 and KMNIST. The gap between the methods grows modestly with increased learning rates and, as theoretically expected, the gap grows faster in the narrow network. On the wide network, across the entire range of learning rates tested, Align-ada outperforms all non-backprop baselines. All methods have a sharp drop in performance at the same learning rate value of 10, at which point training becomes unstable. The effectiveness of Align-ada even at relatively large learning rates contrasts with prior work indicating that wide linearized networks perform best at small learning rates [22]. This discrepancy may be caused by the additional stability arising from only linearizing learning dynamics rather than linearizing the network itself; see Section 4 for further discussion of this difference.

**Varying network width** In Figure 4, we compare performance of different learning rules under architectures of different widths. While Normal performs well at all network widths, Align-ada performs nearly as well as gradient descent at large widths; Align-zero performs worse, but still significantly improves with network width. Align-zero’s relatively worse performance suggests that layers  $\sigma(z_{l-1}^{(t)}(x))$  vary considerably more over the course of training than gradients  $\nabla_{z_l} f^{(t)}(x)$  in finite width networks. At the largest width tested, Align-ada matches or outperforms all baselines except Normal on both CIFAR-10 and KMNIST. Interestingly, on KMNIST, DFA closely tracks the



performance of Align-ada suggesting that DFA’s effectiveness might be partially explained by our theory. See Appendix F for full tabulated results.

**Note on performance** We note that while our accuracies are generally low relative to standardly trained networks, they are in similar ranges to prior results reported for comparably sized networks trained with NTK-based linearized training methods [22]. This validates that our wide networks are indeed trained in a regime approaching the NTK infinite-width limit. It may be possible to improve performance by extending Align-ada and Align-zero to non-NTK regimes via, for example, slow timescale weight transport of backward weights; we leave such extensions as a future work.

## 5.2 Results on Add task

**Dataset and baselines** We train standard ReLU-activated RNNs on the Add task used as a benchmark for biologically-plausible RNN training rules in [29]. Additional details on the dataset, architectures and hyperparameters are included in Appendix E. We compare Align-ada and Align-zero to Normal and Readout-only, which trains only readout weights and fixes all other weights.

**Varying network width** In Figure 5, we plot the training and test set losses of different learning rules. Although we find a large gap between Normal and alignment-based methods at small width, at larger widths, the gap decreases with Align methods performing comparably to Normal at a network scale of 512 hidden units. At large widths, the performance of Align methods far exceed Readout-only training, indicating that tuning the hidden layer representation is useful even at large width when random representations provide enough information to adequately perform the task. See Appendix F for full tabulated results.

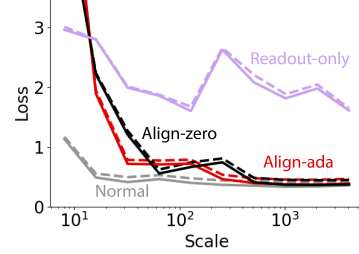


Figure 5: Loss of different learning rules (Normal, Align-ada, Align-zero, Readout-only) as a function of architecture scale on a RNN. Solid lines: test loss; dashed: train loss.

## 5.3 Results on ImageNet

**Dataset and baselines** We train an 8 layer CNN on ImageNet, comparing Align-ada to Normal and FA. Additional details on the dataset, architecture and hyperparameters are included in Appendix E. Our goal is not to achieve competitive performance on ImageNet, but to illustrate that Align-ada can closely match the training dynamics of normal training in the NTK training regime even on challenging real-world datasets.

**Performance during training** In Figure 6, we find that the training loss of Align-ada closely matches that of Normal, with a small gap only emerging after  $1.5 \times 10^5$  training steps. By contrast, FA does not approach the performance of Normal. The results suggest that Align-ada may be significantly more scalable than other backprop-alternative learning rules.

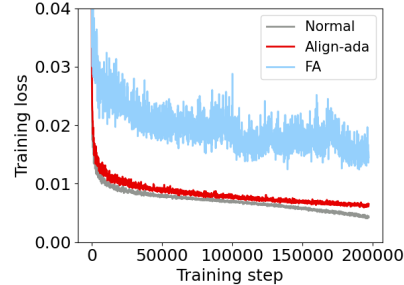


Figure 6: Training loss of different learning rules (Normal, Align-ada, FA) during learning.

## 6 Conclusion

In this paper, we investigated an input-weight alignment effect in wide neural networks in which, through gradient learning, intermediate layer weights align layerwise with error-scaled input correlations. We theoretically proved this alignment effect in NTK infinite-width limit networks and empirically demonstrate it in wide, finite-width networks. Motivated by this finding, we developed two backpropagation-free learning rules designed to produce the same alignment effect. Experiments showed that the learning rules outperform other backpropagation-free learning rules and are comparable to gradient descent in wide, finite-width convolutional and recurrent neural networks under an NTK training regime.

## References

- [1] Chiyuan Zhang, Samy Bengio, Moritz Hardt, Benjamin Recht, and Oriol Vinyals. Understanding deep learning requires rethinking generalization. *ICLR*, 2017.
- [2] Jason Yosinski, Jeff Clune, Yoshua Bengio, and Hod Lipson. How transferable are features in deep neural networks? *NIPS*, 2014.
- [3] Alessio Ansuini, Alessandro Laio, Jakob H. Macke, and Davide Zoccolan. Intrinsic dimension of data representations in deep neural networks. *NeurIPS*, 2019.
- [4] Simon Kornblith, Mohammad Norouzi, Honglak Lee, and Geoffrey Hinton. Similarity of neural network representations revisited. *ICML*, 2019.
- [5] Thao Nguyen, Maithra Raghu, and Simon Kornblith. Do wide and deep networks learn the same things? uncovering how neural network representations vary with width and depth. *ICLR*, 2021.
- [6] Liwei Wang, Lunjia Hu, Jiayuan Gu, Yue Wu, Zhiqiang Hu, Kun He, and John Hopcroft. Towards understanding learning representations: To what extent do different neural networks learn the same representation. *NeurIPS*, 2018.
- [7] Hartmut Maennel, Ibrahim Alabdulmohsin, Ilya Tolstikhin, Robert J. N. Baldock, Olivier Bousquet, Sylvain Gelly, and Daniel Keysers. What Do Neural Networks Learn When Trained With Random Labels? *arXiv preprint*, 2020.
- [8] Andrew M. Saxe, James L. McClelland, and Surya Ganguli. A mathematical theory of semantic development in deep neural networks. *PNAS*, 2019.
- [9] Arthur Jacot, Franck Gabriel, and Clément Hongler. Neural tangent kernel: Convergence and generalization in neural networks. *NIPS*, 2018.
- [10] H Sebastian Seung. Learning in spiking neural networks by reinforcement of stochastic synaptic transmission. *Neuron*, 40(6):1063–1073, 2003.
- [11] I.R. Fiete and H.S. Seung. Gradient learning in spiking neural networks by dynamic perturbation of conductances. *Phys Rev Lett*, 97(4):048104, 2006.
- [12] Yoshua Bengio, Dong-Hyun Lee, Thomas Mesnard Jorg Bornschein, and Zhouhan Lin. Towards biologically plausible deep learning. *arXiv preprint*, 2016.
- [13] Timothy P. Lillicrap, Daniel Cownden, Douglas B. Tweed, and Colin J. Akerman. Random synaptic feedback weights support error backpropagation for deep learning. *Nature Communications*, 2016.
- [14] Arild Nøkland. Direct feedback alignment provides learning in deep neural networks. *NIPS*, 2016.
- [15] Guillaume Bellec, Franz Scherr, Elias Hajek, Darjan Salaj, Robert Legenstein, and Wolfgang Maass. A solution to the learning dilemma for recurrent networks of spiking neurons. *Nature Communications*, 2020.
- [16] Sergey Bartunov, Adam Santoro, Blake A. Richards, Luke Marris, Geoffrey E. Hinton, and Timothy Lillicrap. Assessing the scalability of biologically-motivated deep learning algorithms and architectures. *NIPS*, 2018.
- [17] Blake Richards, Timothy Lillicrap, Philippe Beaudoin, Y. Bengio, Rafal Bogacz, Amelia Christensen, Claudia Clopath, Rui Costa, Archy Berker, Surya Ganguli, Colleen Gillon, Danijar Hafner, Adam Kepecs, Nikolaus Kriegeskorte, Peter Latham, Grace Lindsay, Kenneth Miller, Richard Naud, Christopher Pack, and Konrad Kording. A deep learning framework for neuroscience. *Nature Neuroscience*, 22:1761–1770, 11 2019.
- [18] C. Roth, I. Kanitscheider, and I.R. Fiete. Kernel rnn learning (kernl). In *ICLR*, 2019.
- [19] Alexander G. de G. Matthews, Mark Rowland, Jiri Hron, Richard E. Turner, and Zoubin Ghahramani. Gaussian process behaviour in wide deep neural networks. *ICLR*, 2018.
- [20] Jaehoon Lee, Yasaman Bahri, Roman Novak, Samuel S. Schoenholz, Jeffrey Pennington, and Jascha Sohl-Dickstein. Deep neural networks as gaussian processes. *ICLR*, 2018.
- [21] Sanjeev Arora, Simon S. Du, Wei Hu, Zhiyuan Li, Ruslan Salakhutdinov, and Ruosong Wang. On exact computation with an infinitely wide neural net. *NeurIPS*, 2019.

- [22] Jaehoon Lee, Lechao Xiao, Samuel S. Schoenholz, Yasaman Bahri, Roman Novak, Jascha Sohl-Dickstein, and Jeffrey Pennington. Wide neural networks of any depth evolve as linear models under gradient descent. *NeurIPS*, 2019.
- [23] Jaehoon Lee, Samuel S. Schoenholz, Jeffrey Pennington, Ben Adlam, Lechao Xiao, Roman Novak, and Jascha Sohl-Dickstein. Finite versus infinite neural networks: an empirical study. *NeurIPS*, 2020.
- [24] Greg Yang and Edward J. Hu. Feature learning in infinite-width neural networks. *arXiv preprint*, 2020.
- [25] Arild Nøkland and Lars Hiller Eidnes. Training Neural Networks with Local Error Signals. *ICML*, 2019.
- [26] Alex Krizhevsky. Learning multiple layers of features from tiny images. 2009.
- [27] Tarin Clanuwat, Mikel Bober-Irizar, Asanobu Kitamoto, Alex Lamb, Kazuaki Yamamoto, and David Ha. Deep learning for classical japanese literature. *NeurIPS Workshop on Machine Learning for Creativity and Design*, 2018.
- [28] Olga Russakovsky, Jia Deng, Hao Su, Jonathan Krause, Sanjeev Satheesh, Sean Ma, Zhiheng Huang, Andrej Karpathy, Aditya Khosla, Michael Bernstein, Alexander C. Berg, and Li Fei-Fei. ImageNet Large Scale Visual Recognition Challenge. *IJCV*, 2015.
- [29] Owen Marshell, Kyunghyun Cho, and Cristina Savin. A Unified Framework of Online Learning Algorithms for Training Recurrent Neural Networks. *JMLR*, 2020.
- [30] Roman Novak, Lechao Xiao, Jaehoon Lee, Yasaman Bahri, Greg Yang, Jiri Hron, Daniel A. Abolafia, Jeffrey Pennington, and Jascha Sohl-Dickstein. Bayesian deep convolutional networks with many channels are gaussian processes. *ICLR*, 2019.

## Appendix

### A Proof of Proposition 1

**Proposition 1.** Assume layers are randomly initialized according to the neural tangent initialization [9]. Also, assume that the nonlinearity  $\sigma(\cdot)$  has bounded first and second derivatives. Suppose the network is trained with continuous gradient flow with learning rate  $\eta$  on the mean-squared error loss for  $T$  time such that  $\max_x \|y(x) - f^{(t)}(x)\|_2$  is uniformly bounded in  $t \in [0, T]$ . Then, in the sequential limit  $\lim_{m_{N-1} \rightarrow \infty} \lim_{m_{N-2} \rightarrow \infty} \dots \lim_{m_1 \rightarrow \infty}$ :

$$\frac{1}{\sqrt{m_{l-1}}} \left\| \frac{1}{m_{l-1}} \Sigma_{l, q_l^{(t)}}^{(0)} - \Delta_l^{(t)} \right\|_{op} = 0 \quad (20)$$

*Proof.* Our proof extends Theorem 2 in [9]. We first start with two observations from Theorem 2; in the sequential limit  $\lim_{m_{N-1} \rightarrow \infty} \lim_{m_{N-2} \rightarrow \infty} \dots \lim_{m_1 \rightarrow \infty}$ ,  $\|(W_{N, :, i}^{(t)} - W_{N, :, i}^{(0)})\|_2$  and  $\sqrt{\mathbb{E}_{p_x} [\|z_{N-1, i}^{(t)}(x) - z_{N-1, i}^{(0)}(x)\|_2^2]}$  converge to zero at rates:

$$\|(W_{N, :, i}^{(t)} - W_{N, :, i}^{(0)})\|_2 \in O\left(\frac{1}{\sqrt{m_{N-1}}}\right) \quad (21)$$

$$\sqrt{\mathbb{E}_{p_x} [\|z_{N-1, i}^{(t)}(x) - z_{N-1, i}^{(0)}(x)\|_2^2]} \in O\left(\frac{1}{\sqrt{m_{N-1}}}\right) \quad (22)$$

where  $i$  denotes the elements of  $z_{N-1}$  and columns of  $W_N$ .

Next, we prove by induction that:

$$\lim_{m_{N-1} \rightarrow \infty} \lim_{m_{N-2} \rightarrow \infty} \dots \lim_{m_1 \rightarrow \infty} \sqrt{\mathbb{E}_{p_x} [\|\nabla_{z_l} f_i^{(t)}(x) - \nabla_{z_l} f_i^{(0)}(x)\|_2^2]} = 0$$

for  $l = 1, \dots, N$  at rate  $O(\frac{1}{\sqrt{m_{N-1}}})$ . For the purposes of induction, we assume that instead of training on a mean-squared error loss, the model is trained on a time-varying loss  $L(f^{(t)}(x), y^{(t)}(x))$  such that the following quantity is stochastically bounded:

$$\int_0^T \sqrt{\mathbb{E}[\|d^{(t)}(x)\|_2^2]} \quad (23)$$

where  $d^{(t)}$  satisfies  $\nabla_f \mathbb{E}[L(f(x), y^{(t)}(x))] |_{f^{(t)}(x)} = \mathbb{E}[d^{(t)}(x)^T f(x)]$ . Note that the mean squared error loss satisfies this assumption [9].

First, consider the base case  $N = 1$ . Then,  $\nabla_{z_1} f^{(t)}(x) = \nabla_{z_1} z_1^{(t)}(x) = I = \nabla_{z_1} z_1^{(0)}(x) = \nabla_{z_1} f^{(0)}(x)$ , so the result holds. Next, we apply the inductive hypothesis to the  $N - 1$  layer network starting from the input to layer  $N - 1$

$$\lim_{m_{N-2} \rightarrow \infty} \lim_{m_{N-3} \rightarrow \infty} \dots \lim_{m_1 \rightarrow \infty} \sqrt{\mathbb{E}_{p_x} [\|\nabla_{z_l} z_{N-1, j}^{(t)}(x) - \nabla_{z_l} z_{N-1, j}^{(0)}(x)\|_2^2]} = 0$$

for  $l = 1, \dots, N - 1$ . First, note that as with the base case, the statement holds trivially for  $l = N$  because  $z_N(x) = f(x)$ . For  $l = 1, \dots, N - 1$ , observe that:

$$\begin{aligned} & \sqrt{\mathbb{E}_{p_x} [\|\nabla_{z_l} f_i^{(t)}(x) - \nabla_{z_l} f_i^{(0)}(x)\|_2^2]} \\ &= \frac{1}{\sqrt{m_{N-1}}} \sqrt{\mathbb{E}_{p_x} [\|\nabla_{z_l} z_{N-1}^{(t)}(x) \text{diag}(\sigma'(z_{N-1}^{(t)}(x))) W_{N, :, i}^{(t)T} - \nabla_{z_l} z_{N-1}^{(0)}(x) \text{diag}(\sigma'(z_{N-1}^{(0)}(x))) W_{N, :, i}^{(0)T}\|_2^2]} \\ &\leq \frac{1}{\sqrt{m_{N-1}}} \sqrt{\mathbb{E}_{p_x} [\sum_j \|\nabla_{z_l} z_{N-1}^{(t)}(x)_{:, j} \text{diag}(\sigma'(z_{N-1}^{(t)}(x)))_{j, j} W_{N, j, i}^{(t)T} - \nabla_{z_l} z_{N-1}^{(0)}(x)_{:, j} \text{diag}(\sigma'(z_{N-1}^{(0)}(x)))_{j, j} W_{N, j, i}^{(0)T}\|_2^2]} \end{aligned} \quad (24)$$

Note that in the sequential limit  $\lim_{m_{N-1} \rightarrow \infty} \lim_{m_{N-2} \rightarrow \infty} \dots \lim_{m_1 \rightarrow \infty}$ ,  $\|W_{N, j, i}^{(t)T} - W_{N, j, i}^{(0)T}\|_2^2$  converges to 0 with rate  $O(\frac{1}{m_{N-1}})$ . Similarly, because  $\sigma$  has a bounded second

derivative,  $\mathbb{E}_{p_x}[\|\text{diag}(\sigma'(z_{N-1}^{(t)}(x)))_{j,j} - \text{diag}(\sigma'(z_{N-1}^{(0)}(x)))_{j,j}\|_2^2]$  converges to 0 with rate  $O(\frac{1}{m_{N-1}})$ . Applying the inductive hypothesis, we have that  $\mathbb{E}_{p_x}[\|\nabla_{z_l} f_i^{(t)}(x) - \nabla_{z_l} f_i^{(0)}(x)\|_2^2]$  converges to 0 at rate  $O(\frac{1}{m_{N-1}})$ . Thus,  $\|\nabla_{z_l} z_{N-1}^{(t)}(x)_{:,j} \text{diag}(\sigma'(z_{N-1}^{(t)}(x)))_{j,j} W_{N,j,i}^{(t)T} - \nabla_{z_l} z_{N-1}^{(0)}(x)_{:,j} \text{diag}(\sigma'(z_{N-1}^{(0)}(x)))_{j,j} W_{N,j,i}^{(0)T}\|_2^2$  converges to 0 with rate  $O(\frac{1}{m_{N-1}})$ . After the summation over index  $j$ , this becomes constant. The factor of  $O(\frac{1}{\sqrt{m_{N-1}}})$  implies that  $\sqrt{\mathbb{E}_{p_x}[\|\nabla_{z_l} f_i^{(t)}(x) - \nabla_{z_l} f_i^{(0)}(x)\|_2^2]}$  converges at rate  $O(\frac{1}{\sqrt{m_{N-1}}})$ , completing the proof by induction.

This result implies that  $\mathbb{E}_{p_x}[\|\nabla_{z_l} f^{(t)}(x) - \nabla_{z_l} f^{(0)}(x)\|_{op}]$  also converges to 0 at rate  $O(\frac{1}{\sqrt{m_{N-1}}})$ .

Next, we define  $\tilde{W}^{(t)}$  as:

$$\tilde{W}_l^{(t)} = W_l^{(t)} - W_l^{(0)} - \frac{1}{\sqrt{m_{l-1}}} \eta \mathbb{E}_{p_x}[\nabla_{z_l} f^{(0)}(x) [\int_0^t (y(x) - f^{(\tau)}(x)) d\tau] \sigma(z_{l-1}^{(0)}(x))^T] \quad (25)$$

Note that  $\tilde{W}_l^{(0)} = 0$ . Taking the derivative of both sides:

$$\begin{aligned} \dot{\tilde{W}}_l^{(t)} &= \frac{1}{\sqrt{m_{l-1}}} \eta \mathbb{E}_{p_x}[\nabla_{z_l} f^{(t)}(x) (y(x) - f^{(t)}(x)) \sigma(z_{l-1}^{(t)}(x))^T] \\ &\quad - \frac{1}{\sqrt{m_{l-1}}} \eta \mathbb{E}_{p_x}[\nabla_{z_l} f^{(0)}(x) (y(x) - f^{(t)}(x)) \sigma(z_{l-1}^{(0)}(x))^T] \\ &= \frac{1}{\sqrt{m_{l-1}}} \eta \mathbb{E}_{p_x}[\nabla_{z_l} f^{(t)}(x) (y(x) - f^{(t)}(x)) (\sigma(z_{l-1}^{(t)}(x)) - \sigma(z_{l-1}^{(0)}(x)))^T] \\ &\quad + \frac{1}{\sqrt{m_{l-1}}} \eta \mathbb{E}_{p_x}[(\nabla_{z_l} f^{(t)}(x) - \nabla_{z_l} f^{(0)}(x)) (y(x) - f^{(t)}(x)) \sigma(z_{l-1}^{(0)}(x))^T] \quad (26) \end{aligned}$$

Bounding the norm of  $\dot{\tilde{W}}_l^{(t)}$ :

$$\begin{aligned} \|\dot{\tilde{W}}_l^{(t)}\|_{op} &\leq \frac{1}{\sqrt{m_{l-1}}} \eta \mathbb{E}_{p_x}[\|\nabla_{z_l} f^{(t)}(x) (y(x) - f^{(t)}(x)) (\sigma(z_{l-1}^{(t)}(x)) - \sigma(z_{l-1}^{(0)}(x)))^T\|_{op}] \\ &\quad + \frac{1}{\sqrt{m_{l-1}}} \eta \mathbb{E}_{p_x}[\|(\nabla_{z_l} f^{(t)}(x) - \nabla_{z_l} f^{(0)}(x)) (y(x) - f^{(t)}(x)) \sigma(z_{l-1}^{(0)}(x))^T\|_{op}] \\ &\leq \frac{1}{\sqrt{m_{l-1}}} \eta \mathbb{E}_{p_x}[\|\nabla_{z_l} f^{(t)}(x)\|_{op} \|y(x) - f^{(t)}(x)\|_2 \|\sigma(z_{l-1}^{(t)}(x)) - \sigma(z_{l-1}^{(0)}(x))\|_2] \\ &\quad + \frac{1}{\sqrt{m_{l-1}}} \eta \mathbb{E}_{p_x}[\|\nabla_{z_l} f^{(t)}(x) - \nabla_{z_l} f^{(0)}(x)\|_{op} \|y(x) - f^{(t)}(x)\|_2 \|\sigma(z_{l-1}^{(0)}(x))\|_2] \\ &\leq c\eta \max_x \|\nabla_{z_l} f^{(t)}(x)\|_{op} \max_x \|y(x) - f^{(t)}(x)\|_2 \mathbb{E}_{p_x}[\|\frac{1}{\sqrt{m_{l-1}}} (z_{l-1}^{(t)}(x) - z_{l-1}^{(0)}(x))\|_2] \\ &\quad + \eta \mathbb{E}_{p_x}[\|\nabla_{z_l} f^{(t)}(x) - \nabla_{z_l} f^{(0)}(x)\|_{op}] \max_x \|y(x) - f^{(t)}(x)\|_2 \max_x \|\frac{1}{\sqrt{m_{l-1}}} \sigma(z_{l-1}^{(0)}(x))\|_2 \quad (27) \end{aligned}$$

where  $c$  is the Lipschitz constant of  $\sigma$ . Next, observe that  $\max_{t \in [0, T]} \max_x \|\nabla_{z_l} f^{(t)}(x)\|_{op}$  and  $\max_{t \in [0, T]} \max_x \|\frac{1}{\sqrt{m_{l-1}}} \sigma(z_{l-1}^{(0)}(x))\|_2$  are bounded in the sequential limit  $\lim_{m_{N-1} \rightarrow \infty} \lim_{m_{N-2} \rightarrow \infty} \dots \lim_{m_1 \rightarrow \infty}$ . Moreover,  $\mathbb{E}_{p_x}[\|\frac{1}{\sqrt{m_{l-1}}} (z_{l-1}^{(t)}(x) - z_{l-1}^{(0)}(x))\|_2]$  and  $\mathbb{E}_{p_x}[\|\nabla_{z_l} f^{(t)}(x) - \nabla_{z_l} f^{(0)}(x)\|_{op}]$  approach 0 in this limit. Since  $\max_x \|y(x) - f^{(t)}(x)\|_2$  is uniformly bounded in  $t \in [0, T]$  by assumption,  $\max_{t \in [0, T]} \|\dot{\tilde{W}}_l^{(t)}\|_{op}$  approaches 0 in this limit. Thus,

$$\begin{aligned} \lim_{m_{N-1} \rightarrow \infty} \lim_{m_{N-2} \rightarrow \infty} \dots \lim_{m_1 \rightarrow \infty} \|\dot{\tilde{W}}_l^{(t)}\|_{op} &\leq \lim_{m_{N-1} \rightarrow \infty} \lim_{m_{N-2} \rightarrow \infty} \dots \lim_{m_1 \rightarrow \infty} \int_0^t \|\dot{\tilde{W}}_l^{(\tau)}\|_{op} d\tau \\ &\leq \int_0^t \lim_{m_{N-1} \rightarrow \infty} \lim_{m_{N-2} \rightarrow \infty} \dots \lim_{m_1 \rightarrow \infty} \|\dot{\tilde{W}}_l^{(\tau)}\|_{op} d\tau = 0 \quad (28) \end{aligned}$$

Next, observe that:

$$\begin{aligned}\Sigma_{l,q_l^{(t)}}^{(0)} &= \mathbb{E}_{x_1 \sim p_x, x_2 \sim p_x} [\sigma(z_{l-1}^{(0)}(x_1)) \delta^{(t)}(x_1)^T \nabla_{z_l} f^{(0)}(x_1)^T \nabla_{z_l} f^{(0)}(x_2) \delta^{(t)}(x_2) \sigma(z_{l-1}^{(0)}(x_2))^T] \\ &= m_{l-1} (W_l^{(t)} - W_l^{(0)} - \tilde{W}_l^{(0)})^T (W_l^{(t)} - W_l^{(0)} - \tilde{W}_l^{(0)})\end{aligned}\quad (29)$$

This implies:

$$\begin{aligned}& \frac{1}{\sqrt{m_{l-1}}} \left\| \frac{1}{m_{l-1}} \Sigma_{l,q_l^{(t)}}^{(0)} - \Delta_l^{(t)} \right\|_{op} \\ &= \frac{1}{\sqrt{m_{l-1}}} \left\| (W_l^{(t)} - W_l^{(0)} - \tilde{W}_l^{(0)})^T (W_l^{(t)} - W_l^{(0)} - \tilde{W}_l^{(0)}) - (W_l^{(t)} - W_l^{(0)})^T (W_l^{(t)} - W_l^{(0)}) \right\|_{op} \\ &\leq 2 \frac{1}{\sqrt{m_{l-1}}} \left\| (W_l^{(t)} - W_l^{(0)}) \right\|_{op} \left\| \tilde{W}_l^{(0)} \right\|_{op} + \frac{1}{\sqrt{m_{l-1}}} \left\| \tilde{W}_l^{(0)T} \tilde{W}_l^{(0)} \right\|_{op}\end{aligned}\quad (30)$$

Finally, note that  $\frac{1}{\sqrt{m_{l-1}}} \left\| (W_l^{(t)} - W_l^{(0)}) \right\|_{op}$  converges to 0. Combining this with the convergence of  $\left\| \tilde{W}_l^{(0)} \right\|_{op}$  to 0, we find that  $\frac{1}{\sqrt{m_{l-1}}} \left\| \frac{1}{m_{l-1}} \Sigma_{l,q_l^{(t)}}^{(0)} - \Delta_l^{(t)} \right\|_{op}$  also converges to 0.  $\square$

**Interpretation of the width scaling in Proposition 1** Observe that as network width approaches infinity, both weights and intermediate layer activations change vanishingly over the course of training. Thus, the corresponding correlation matrices  $\Delta_l^{(t)}$  and  $\Sigma_{l,q_l^{(t)}}^{(0)}$  also approach zero under the appropriate width-dependent normalizations. In light of this, it is important to consider whether Proposition 1 really shows an alignment effect between  $\Delta_l^{(t)}$  and  $\Sigma_{l,q_l^{(t)}}^{(0)}$  or merely holds because the correlation matrices individually approach zero.

Note that since  $\left\| W_l^{(t)} - W_l^{(0)} \right\|_{op}$  grows as  $o(\sqrt{m_{l-1}})$ ,  $\frac{1}{\sqrt{m_{l-1}}} \left\| \Delta_l^{(t)} \right\|_{op}$  also grows as  $o(\sqrt{m_{l-1}})$ , which will generally *not* converge to 0. Similarly,  $\left\| \sigma(z_{l-1}^{(0)}(x)) \right\|_2$  grows as  $O(m_{l-1})$ , implying  $\frac{1}{\sqrt{m_{l-1}}} \left\| \frac{1}{m_{l-1}} \Sigma_{l,q_l^{(t)}}^{(0)} \right\|_{op}$  grows as  $O(\sqrt{m_{l-1}})$ . Thus, neither term in the Proposition 1 expression individually approaches zero, and the result does not trivially follow from the individual terms separately approaching zero. Therefore, the convergence of the norm difference in Proposition 1 demonstrates that the two correlation matrices point in the same direction away from the origin and indeed can be interpreted as an alignment effect.

## B Proof of Proposition 2

**Proposition 2** Assume layers are randomly initialized according to the neural tangent initialization [9]. Also, assume that the nonlinearity  $\sigma(\cdot)$  has bounded first and second derivatives. Suppose all methods use learning rate  $\eta$  on the mean-squared error loss for  $T$  time such that  $\max_x \|y(x) - f^{(t)}(x)\|_2$  is uniformly bounded in  $t \in [0, T]$ . Then, in the sequential limit  $\lim_{m_{N-1} \rightarrow \infty} \lim_{m_{N-2} \rightarrow \infty} \dots \lim_{m_1 \rightarrow \infty}$ :

$$f^{(t)}(x) = f_{al,0}^{(t)}(x) = f_{al,ada}^{(t)}(x) \quad (31)$$

*Proof.* First, note that  $f^{(t)}(x)$  evolves as:

$$\dot{f}^{(t)}(x) = \eta \nabla_{\theta} f^{(t)}(x)^T \mathbb{E}[\nabla_{\theta} f^{(t)}(x)(y(x) - f^{(t)}(x))] \quad (32)$$

where  $\theta$  are the parameters of  $f^{(t)}$ . The term in expectation corresponds to the gradient of the total loss (over all points) with respect to the network parameters  $\theta$ , while  $\nabla_{\theta} f^{(t)}(x)^T$  indicates how parameter changes affect the value of  $f^{(t)}$  evaluated at point  $x$ .

We consider a general alternative learning procedure that trains a network  $f_*^{(t)}$  which replaces the feedback Jacobian  $\nabla_{\theta} f^{(t)}(x)$  with a general function  $J_*^{(t)}(x)$ .  $f_*^{(t)}$  evolves as:

$$\dot{f}_*^{(t)}(x) = \eta \nabla_{\theta} f_*^{(t)}(x)^T \mathbb{E}[J_*^{(t)}(x)(y(x) - f_*^{(t)}(x))] \quad (33)$$

Note that here, parameter changes, corresponding to the term in expectation, depend on  $J_*^{(t)}(x)$  and not on the true feedback Jacobian  $\nabla_\theta f_*^{(t)}(x)$ . Thus, in general, the above rule avoids exact backpropagation. However, parameter changes affect the network output according to the true feedback Jacobian  $\nabla_\theta f_*^{(t)}(x)$ .

Define  $\Delta_1^{(t)}(x) = \nabla_\theta f_*^{(t)}(x) - \nabla_\theta f^{(t)}(x)$  and  $\Delta_2^{(t)}(x) = J_*^{(t)}(x) - \nabla_\theta f^{(t)}(x)$ . Next, finding the difference of  $\dot{f}^{(t)}(x)$  and  $\dot{f}_*^{(t)}(x)$ :

$$\begin{aligned}
\dot{f}_*^{(t)}(x) - \dot{f}^{(t)}(x) &= \eta \nabla_\theta f_*^{(t)}(x)^T \mathbb{E}[J_*^{(t)}(x)(y(x) - f_*^{(t)}(x))] - \eta \nabla_\theta f^{(t)}(x)^T \mathbb{E}[\nabla_\theta f^{(t)}(x)(y(x) - f^{(t)}(x))] \\
&= \eta \nabla_\theta f_*^{(t)}(x)^T \mathbb{E}[J_*^{(t)}(x)(y(x) - f^{(t)}(x))] - \eta \nabla_\theta f^{(t)}(x)^T \mathbb{E}[\nabla_\theta f^{(t)}(x)(y(x) - f^{(t)}(x))] \\
&\quad + \eta \nabla_\theta f_*^{(t)}(x)^T \mathbb{E}[J_*^{(t)}(x)(f^{(t)}(x) - f_*^{(t)}(x))] \\
&= \eta \nabla_\theta f^{(t)}(x)^T \mathbb{E}[J_*^{(t)}(x)(y(x) - f^{(t)}(x))] - \eta \nabla_\theta f^{(t)}(x)^T \mathbb{E}[\nabla_\theta f^{(t)}(x)(y(x) - f^{(t)}(x))] \\
&\quad + \eta \Delta_1^{(t)}(x)^T \mathbb{E}[J_*^{(t)}(x)(y(x) - f^{(t)}(x))] + \eta \nabla_\theta f_*^{(t)}(x)^T \mathbb{E}[J_*^{(t)}(x)(f^{(t)}(x) - f_*^{(t)}(x))] \\
&= \eta \Delta_1^{(t)}(x)^T \mathbb{E}[(\nabla_\theta f^{(t)}(x) + \Delta_2^{(t)}(x))(y(x) - f^{(t)}(x))] + \eta \nabla_\theta f^{(t)}(x)^T \mathbb{E}[\Delta_2^{(t)}(x)(y(x) - f^{(t)}(x))] \\
&\quad + \eta (\nabla_\theta f^{(t)}(x) + \Delta_1^{(t)}(x))^T \mathbb{E}[(\nabla_\theta f^{(t)}(x) + \Delta_2^{(t)}(x))(f^{(t)}(x) - f_*^{(t)}(x))] \quad (34)
\end{aligned}$$

Bounding the derivative of the discrepancy between  $f^{(t)}(x)$  and  $f_*^{(t)}(x)$ :

$$\begin{aligned}
\frac{d}{dt} \|f_*^{(t)}(x) - f^{(t)}(x)\|_2 &\leq \|\dot{f}_*^{(t)}(x) - \dot{f}^{(t)}(x)\|_2 \\
&\leq \eta \max_x \|\Delta_1^{(t)}(x)\|_{op} (\max_x \|\nabla_\theta f^{(t)}(x)\|_{op} + \max_x \|\Delta_2^{(t)}(x)\|_{op}) \max_x \|y(x) - f^{(t)}(x)\|_2 \\
&\quad + \eta \max_x \|\nabla_\theta f^{(t)}(x)\|_{op} \max_x \|\Delta_2^{(t)}(x)\|_{op} \max_x \|y(x) - f^{(t)}(x)\|_2 \\
&+ \eta (\max_x \|\nabla_\theta f^{(t)}(x)\|_{op} + \max_x \|\Delta_1^{(t)}(x)\|_{op}) (\max_x \|\nabla_\theta f^{(t)}(x)\|_{op} + \max_x \|\Delta_2^{(t)}(x)\|_{op}) \max_x \|f^{(t)}(x) - f_*^{(t)}(x)\|_2 \quad (35)
\end{aligned}$$

Taking the integral of both sides:

$$\begin{aligned}
&\|f_*^{(t)}(x) - f^{(t)}(x)\|_2 \\
&\leq \int_0^t \eta \max_x \|\Delta_1^{(\tau)}(x)\|_{op} (\max_x \|\nabla_\theta f^{(\tau)}(x)\|_{op} + \max_x \|\Delta_2^{(\tau)}(x)\|_{op}) \max_x \|y(x) - f^{(\tau)}(x)\|_2 d\tau \\
&\quad + \int_0^t \eta \max_x \|\nabla_\theta f^{(\tau)}(x)\|_{op} \max_x \|\Delta_2^{(\tau)}(x)\|_{op} \max_x \|y(x) - f^{(\tau)}(x)\|_2 d\tau \\
&+ \eta (\max_x \|\nabla_\theta f^{(t)}(x)\|_{op} + \max_x \|\Delta_1^{(t)}(x)\|_{op}) (\max_x \|\nabla_\theta f^{(t)}(x)\|_{op} + \max_x \|\Delta_2^{(t)}(x)\|_{op}) \max_x \|f^{(t)}(x) - f_*^{(t)}(x)\|_2 \quad (36)
\end{aligned}$$

Define

$$\begin{aligned}
\alpha(t) &= \int_0^t \eta \max_x \|\Delta_1^{(\tau)}(x)\|_{op} (\max_x \|\nabla_\theta f^{(\tau)}(x)\|_{op} + \max_x \|\Delta_2^{(\tau)}(x)\|_{op}) \max_x \|y(x) - f^{(\tau)}(x)\|_2 d\tau \\
&\quad + \int_0^t \eta \max_x \|\nabla_\theta f^{(\tau)}(x)\|_{op} \max_x \|\Delta_2^{(\tau)}(x)\|_{op} \max_x \|y(x) - f^{(\tau)}(x)\|_2 d\tau \quad (37)
\end{aligned}$$

$$\beta(t) = \eta (\max_x \|\nabla_\theta f^{(t)}(x)\|_{op} + \max_x \|\Delta_1^{(t)}(x)\|_{op}) (\max_x \|\nabla_\theta f^{(t)}(x)\|_{op} + \max_x \|\Delta_2^{(t)}(x)\|_{op}) \quad (38)$$

$$u(t) = \max_x \|f_*^{(t)}(x) - f^{(t)}(x)\|_2 \quad (39)$$

Then, the above inequality implies:

$$u(t) \leq \alpha(t) + \int_0^t \beta(\tau) u(\tau) d\tau \quad (40)$$

By Grönwall's inequality:

$$u(t) \leq \alpha(t) \exp \left( \int_0^t \beta(\tau) d\tau \right) \quad (41)$$

Finally, observe that if in the sequential limit  $\lim_{m_{N-1} \rightarrow \infty} \lim_{m_{N-2} \rightarrow \infty} \dots \lim_{m_1 \rightarrow \infty}$ ,  $\max_x \|\Delta_1^{(t)}(x)\|_{op}$  and  $\max_x \|\Delta_2^{(t)}(x)\|_{op}$  converge uniformly to 0 in range  $[0, T]$ , then, in the same limit,  $\alpha(t)$  converges to 0 implying  $u(t)$  converges to 0. Thus, if  $\max_x \|\Delta_1^{(t)}(x)\|_{op}$  and  $\max_x \|\Delta_2^{(t)}(x)\|_{op}$  uniformly converge to 0, then  $f^{(t)}(x) = f_*(x)$ .

Next, we show that  $\max_x \|\Delta_1^{(t)}(x)\|_{op}$  and  $\max_x \|\Delta_2^{(t)}(x)\|_{op}$  uniformly converge to 0 for Align-zero and Align-ada. We first adapt Lemma 1 of [9] to show that weights and intermediate layer activations of Align-zero and Align-ada networks do not change over the course of training in the sequential limit  $\lim_{m_{N-1} \rightarrow \infty} \lim_{m_{N-2} \rightarrow \infty} \dots \lim_{m_1 \rightarrow \infty}$ .

Define  $a_l^{(t)} = \sqrt{\mathbb{E}[\|\frac{1}{\sqrt{m_l}} z_l^{(t)}(x)\|_2^2]}$ ,  $w_l^{(t)} = \|\frac{1}{\sqrt{m_{l-1}}} W_l^{(t)}\|_{op}$ ,  $\tilde{a}_l^{(t)} = \sqrt{\mathbb{E}[\|\frac{1}{\sqrt{m_l}} z_l^{(t)}(x) - \frac{1}{\sqrt{m_l}} z_l^{(0)}(x)\|_2^2]}$ ,  $\tilde{w}_l^{(t)} = \|\frac{1}{\sqrt{m_{l-1}}} W_l^{(t)} - \frac{1}{\sqrt{m_{l-1}}} W_l^{(0)}\|_{op}$ , where  $W_l^{(t)}$  and  $z_l^{(t)}(x)$  represent the weights and layers of the Align-zero or Align-ada network. Note that the derivatives of  $\tilde{w}_l^{(t)}$  can be bounded as:

$$\dot{\tilde{w}}_l^{(t)} \leq \left\| \frac{1}{\sqrt{m_{l-1}}} \dot{W}_l^{(t)} \right\|_{op} \leq \frac{1}{\sqrt{m_{l-1}}} \mathcal{P}(a_{l-1}^{(0)}, a_{l-1}^{(t)}, w_{l+1}^{(0)}, w_{l+2}^{(0)}, \dots, w_N^{(0)}) \max_x \|y(x) - f^{(t)}(x)\|_2 \quad (42)$$

where  $\mathcal{P}$  is a polynomial with positive coefficients not depending on the width of any layers in the network. Similarly, the derivatives of  $\tilde{a}_l^{(t)}$  can be bounded as:

$$\dot{\tilde{a}}_l^{(t)} \leq \frac{1}{\sqrt{m_l}} \mathcal{P}(a_0^{(0)}, a_0^{(t)}, \dots, a_{l-1}^{(0)}, a_{l-1}^{(t)}, w_1^{(0)}, w_1^{(t)}, \dots, w_l^{(0)}, w_l^{(t)}, w_{l+1}^{(0)}, w_{l+2}^{(0)}, \dots, w_N^{(0)}) \max_x \|y(x) - f^{(t)}(x)\|_2 \quad (43)$$

where  $\mathcal{P}$  is another polynomial with positive coefficients not depending on the width of any layers in the network. Next, define  $A(t)$  as:

$$\sum_{l=0}^{N-1} a_l^{(0)} + \tilde{a}_l^{(t)} + w_{l+1}^{(0)} + \tilde{w}_{l+1}^{(t)} \quad (44)$$

Observe that using the previous bounds on  $\dot{\tilde{w}}_l^{(t)}$  and  $\dot{\tilde{a}}_l^{(t)}$ , the derivative of  $A(t)$  can be bounded as:

$$\frac{d}{dt} A(t) \leq \frac{1}{\sqrt{\min\{m_1, \dots, m_{N-1}\}}} \mathcal{P}(A(t)) \max_x \|y(x) - f^{(t)}(x)\|_2 \quad (45)$$

where  $\mathcal{P}$  is a polynomial. Finally, observe that  $A(0)$  is stochastically bounded as it is only a function of  $a_l^{(0)}$  and  $w_l^{(0)}$ . By Grönwall's inequality, we find that  $A(t)$  can be uniformly bounded in an interval  $[0, \tau]$ , with  $\tau$  approaching  $T$  as  $\min\{m_1, \dots, m_{N-1}\} \rightarrow \infty$ . This implies  $\mathcal{P}(A(t))$  can be uniformly bounded in this interval. Recall also our assumption that  $\max_x \|y(x) - f^{(t)}(x)\|_2$  is also uniformly bounded in this interval. Then, due to the  $\frac{1}{\sqrt{\min\{m_1, \dots, m_{N-1}\}}}$  coefficient in the bound for  $\frac{d}{dt} A(t)$ ,

in the sequential limit  $\lim_{m_{N-1} \rightarrow \infty} \lim_{m_{N-2} \rightarrow \infty} \dots \lim_{m_1 \rightarrow \infty}$ ,  $\frac{d}{dt} A(t)$  converges uniformly to 0 in any interval  $[0, \tau]$  where  $\tau < T$ . Thus,  $A(t) = A(0)$  in this limit. Therefore, in the sequential limit  $\lim_{m_{N-1} \rightarrow \infty} \lim_{m_{N-2} \rightarrow \infty} \dots \lim_{m_1 \rightarrow \infty}$ ,  $\tilde{a}_l^{(t)}$  and  $\tilde{w}_l^{(t)}$  converge uniformly to 0 in  $[0, T]$ . Note that this convergence holds for both Align-zero and Align-ada, in addition to normal training by gradient descent (see [9]).

Next, we bound  $\max_x \|\Delta_1^{(t)}(x)\|_{op}$  and  $\max_x \|\Delta_2^{(t)}(x)\|_{op}$  in terms of  $\tilde{a}_l^{(t)}$  and  $\tilde{w}_l^{(t)}$ . Observe that:

$$\max_x \|\Delta_1^{(t)}(x)\|_{op} \leq \max_x \|\nabla_\theta f_*(x) - \nabla_\theta f^{(0)}(x)\|_{op} + \max_x \|\nabla_\theta f^{(t)}(x) - \nabla_\theta f^{(0)}(x)\|_{op} \quad (46)$$

and

$$\max_x \|\Delta_2^{(t)}(x)\|_{op} \leq \max_x \|J_*^{(t)}(x) - \nabla_\theta f^{(0)}(x)\|_{op} + \max_x \|\nabla_\theta f^{(t)}(x) - \nabla_\theta f^{(0)}(x)\|_{op} \quad (47)$$



First, note that since  $\nabla_{\theta} f^{(t)}(x)$  is a function of weights and intermediate layer activations at time  $t$ :

$$\begin{aligned} \max_x \|\nabla_{\theta} f^{(t)}(x) - \nabla_{\theta} f^{(0)}(x)\|_{op} &\leq \sum_{l=1}^N \tilde{w}_l^{(t)} \mathcal{P}_{w,l}(a_0^{(0)}, a_0^{(t)}, \dots, a_{N-1}^{(0)}, a_{N-1}^{(t)}, w_1^{(0)}, w_1^{(t)}, \dots, w_N^{(0)}, w_N^{(t)}) \\ &\quad + \sum_{l=0}^{N-1} \tilde{a}_l^{(t)} \mathcal{P}_{a,l}(a_0^{(0)}, a_0^{(t)}, \dots, a_{N-1}^{(0)}, a_{N-1}^{(t)}, w_1^{(0)}, w_1^{(t)}, \dots, w_N^{(0)}, w_N^{(t)}) \end{aligned} \quad (48)$$

where  $\mathcal{P}_{w,l}$  and  $\mathcal{P}_{a,l}$  are polynomials with positive coefficients not depending on any layer's width and  $a_l^{(t)}$ ,  $\tilde{a}_l^{(t)}$  and  $w_l^{(t)}$ ,  $\tilde{w}_l^{(t)}$  are found on network  $f^{(t)}(x)$ . This is because the time-variation of the gradient of any parameter in the network is constrained either by the variation in a weight  $\tilde{w}_l^{(t)}$  or variation in a layer's activations  $\tilde{a}_l^{(t)}$ . Similarly,

$$\begin{aligned} \max_x \|\nabla_{\theta} f_*^{(t)}(x) - \nabla_{\theta} f^{(0)}(x)\|_{op} &\leq \sum_{l=1}^N \tilde{w}_l^{(t)} \mathcal{P}_{w,l}(a_0^{(0)}, a_0^{(t)}, \dots, a_{N-1}^{(0)}, a_{N-1}^{(t)}, w_1^{(0)}, w_1^{(t)}, \dots, w_N^{(0)}, w_N^{(t)}) \\ &\quad + \sum_{l=0}^{N-1} \tilde{a}_l^{(t)} \mathcal{P}_{a,l}(a_0^{(0)}, a_0^{(t)}, \dots, a_{N-1}^{(0)}, a_{N-1}^{(t)}, w_1^{(0)}, w_1^{(t)}, \dots, w_N^{(0)}, w_N^{(t)}) \end{aligned} \quad (49)$$

where now  $a_l^{(t)}$ ,  $\tilde{a}_l^{(t)}$  and  $w_l^{(t)}$ ,  $\tilde{w}_l^{(t)}$  are found on network  $f_*^{(t)}(x)$ . Finally,

$$\max_x \|J_*^{(t)}(x) - \nabla_{\theta} f^{(0)}(x)\|_{op} \leq \sum_{l=0}^{N-1} \tilde{a}_l^{(t)} \mathcal{P}_l(w_1^{(0)}, \dots, w_N^{(0)}) \quad (50)$$

where we find a simpler expression without  $\tilde{w}_l^{(t)}$  because the layerwise Jacobian  $\nabla_{z_l} f^{(0)}(x)$ , which only depends on time 0 parameter values, is used to send feedback in both Align-zero and Align-ada. For Align-ada  $\tilde{a}_l^{(t)}$  appears in the bound because  $\|J_*^{(t)}(x) - \nabla_{\theta} f^{(0)}(x)\|_{op}$  depends on both constant-over-time layerwise Jacobian  $\nabla_{z_l} f^{(0)}(x)$  and time varying activations  $\sigma(z_l^{(t)}(x))$  which have variations bounded by  $\tilde{a}_l^{(t)}$ . Note that the bound is 0 for Align-zero since  $J_*^{(t)}(x) = \nabla_{\theta} f^{(0)}(x)$ .

Using these bounds and the fact that  $\tilde{a}_l^{(t)}$  and  $\tilde{w}_l^{(t)}$  converge uniformly to zero in  $[0, T]$  in the sequential infinite-width limit, we find that in the same limit,  $\max_x \|\Delta_1^{(t)}(x)\|_{op}$  and  $\max_x \|\Delta_2^{(t)}(x)\|_{op}$  also converge uniformly to 0 in  $[0, T]$ . Therefore, we find that in the limit  $\lim_{m_{N-1} \rightarrow \infty} \lim_{m_{N-2} \rightarrow \infty} \dots \lim_{m_1 \rightarrow \infty}$ :

$$f^{(t)}(x) = f_{al,0}^{(t)}(x) = f_{al-ada}^{(t)}(x) \quad (51)$$

□

## C Pseudocode for Align-zero and Align-ada

---

### Algorithm 1 Align-zero training

---

**Require:** Training points  $\mathcal{X}$ , training steps  $T$ , layer widths  $m_1, m_2, \dots, m_L$ , learning rate  $\eta$

Initialize weights  $W_1^{(0)}, b_1^{(0)}, \dots, W_N^{(0)}, b_N^{(0)}$   
**for** Mini-batch  $x \in \mathcal{X}$  **do**  
  **for**  $l = 1, \dots, N$  **do**  
     $z_l^{(0)}(x) = \frac{1}{\sqrt{m_{l-1}}} W_l^{(0)} \sigma(z_{l-1}^{(0)}(x)) + b_l^{(0)}$   
  **end for**  
   $g_N(x) = I$  // Finding  $\nabla_{z_l} f^{(0)}(x)$   
  **for**  $l = N - 1, \dots, 1$  **do**  
     $g_l(x) = \text{diag}(\sigma'(z_l^{(0)}(x))) \frac{1}{\sqrt{m_l}} W_{l+1}^T g_{l+1}(x)$   
  **end for**  
**end for**  
**for**  $t = 1, \dots, T$  **do**  
  Sample mini-batch  $x \in \mathcal{X}$   
  **for**  $l = 1, \dots, N$  **do**  
     $z_l^{(t-1)}(x) = \frac{1}{\sqrt{m_{l-1}}} W_l^{(t-1)} \sigma(z_{l-1}^{(t-1)}(x)) + b_l^{(t-1)}$   
  **end for**  
   $W_l^{(t)} = W_l^{(t-1)} + \frac{\eta}{\sqrt{m_{l-1}}} g_l(x) \nabla_{z_N(x)} L(z_N^{(t-1)}(x), y(x)) \sigma(z_{l-1}^{(0)}(x))^T$   
   $b_l^{(t)} = b_l^{(t-1)} + \eta g_l(x) \nabla_{z_N(x)} L(z_N^{(t-1)}(x), y(x))$   
**end for**  
Return  $W_1^{(T)}, b_1^{(T)}, \dots, W_N^{(T)}, b_N^{(T)}$

---



---

### Algorithm 2 Align-ada training

---

**Require:** Training points  $\mathcal{X}$ , training steps  $T$ , layer widths  $m_1, m_2, \dots, m_L$ , learning rate  $\eta$

Initialize weights  $W_1^{(0)}, b_1^{(0)}, \dots, W_N^{(0)}, b_N^{(0)}$   
**for** Mini-batch  $x \in \mathcal{X}$  **do**  
  **for**  $l = 1, \dots, N$  **do**  
     $z_l^{(0)}(x) = \frac{1}{\sqrt{m_{l-1}}} W_l^{(0)} \sigma(z_{l-1}^{(0)}(x)) + b_l^{(0)}$   
  **end for**  
   $g_N(x) = I$  // Finding  $\nabla_{z_l} f^{(0)}(x)$   
  **for**  $l = N - 1, \dots, 1$  **do**  
     $g_l(x) = \text{diag}(\sigma'(z_l^{(0)}(x))) \frac{1}{\sqrt{m_l}} W_{l+1}^T g_{l+1}(x)$   
  **end for**  
**end for**  
**for**  $t = 1, \dots, T$  **do**  
  Sample mini-batch  $x \in \mathcal{X}$   
  **for**  $l = 1, \dots, N$  **do**  
     $z_l^{(t-1)}(x) = \frac{1}{\sqrt{m_{l-1}}} W_l^{(t-1)} \sigma(z_{l-1}^{(t-1)}(x)) + b_l^{(t-1)}$   
  **end for**  
   $W_l^{(t)} = W_l^{(t-1)} + \frac{\eta}{\sqrt{m_{l-1}}} g_l(x) \nabla_{z_N(x)} L(z_N^{(t-1)}(x), y(x)) \sigma(z_{l-1}^{(t-1)}(x))^T$   
   $b_l^{(t)} = b_l^{(t-1)} + \eta g_l(x) \nabla_{z_N(x)} L(z_N^{(t-1)}(x), y(x))$   
**end for**  
Return  $W_1^{(T)}, b_1^{(T)}, \dots, W_N^{(T)}, b_N^{(T)}$

---

## D Implementation of Align-zero and Align-ada in recurrent neural networks

Although throughout this paper we use the notation of feedforward neural networks, note that our analysis applies to recurrent neural networks as well since RNNs produce feedforward networks when unrolled over time. For example, in the notation of feedforward networks,  $z_l(x)$  would refer

to the pre-activated hidden state of the network at time step  $l$  of recurrent processing. However, there are typically three key differences with the feedforward case: 1) losses  $L(\hat{y}_l(x), y_l(x))$  can be accumulated over different time steps where  $\hat{y}_l(x)$  is the predicted label depending on state  $z_l(x)$ , 2) inputs can be fed in at different time steps, 3) that recurrent weights and biases are tied at all time-steps (i.e.  $W = W_1 = W_2 = \dots; b = b_1 = b_2 = \dots$ ), although these weights can change over the course of training. Thus, parameter updates must be summed over all losses and all recurrent time-steps where the parameters are applied. The resulting Align-ada learning rule for the recurrent weights of an RNN is:

$$\dot{W}_{al-ada}^{(t)} = \frac{\eta}{\sqrt{m}} \times \sum_{i,j:j>i} \mathbb{E}_{p_x} [\nabla_{z_i} \hat{y}_j^{(0)}(x) \nabla_{\hat{y}_j} L(\hat{y}_j^{(t)}(x), y_j(x)) \sigma(z_{i-1}^{(t)}(x))^T] \quad (52)$$

The learning rules for other parameters (i.e. biases, readout-weights, etc.) can be found similarly, and the adaptation of the Align-zero learning rule can be found analogously.

## E Implementation details

All experiments are run on an Nvidia Tesla K20Xm GPU.

**CIFAR-10 experiments** We train on CNN architecture with 7 convolutional layers followed by global average pooling and a fully connected layer. All convolutional layers use 3-by-3 convolutions with the same number of filters, which is varied from 8 to 512. All but the 4th and 6th convolutional layers have stride 1-by-1, with the other two using stride 2-by-2. All convolution layers are followed by batch normalization and a ReLU non-linearity. Networks are trained on a mean squared error loss. Following [30], labels are constructed as one hot encoded labels minus 0.1 so that they have mean 0. Images are scaled in range  $[0, 1]$ . For each training method, test set accuracies are evaluated at each training epoch, and the best results reported. A learning rate grid search in  $\{1, 2, 5\}$  is performed for all training methods and the best result reported unless otherwise mentioned. See our experiments varying learning rate for observations on training instability beyond a learning rate of 5. We use a batch size of 100, and all methods are trained for 150 epochs unless otherwise mentioned.

**KMNIST experiments** We train on CNN architecture with 3 convolutional layers followed by global average pooling and a fully connected layer. All convolutional layers use 3-by-3 convolutions with the same number of filters, which is varied from 8 to 512. The first layer uses stride 1-by-1, with the other two using stride 2-by-2. All convolution layers are followed by batch normalization and a ReLU non-linearity. Networks are trained on a mean squared error loss. Following [30], labels are constructed as one hot encoded labels minus 0.1 so that they have mean 0. Images are scaled in range  $[0, 1]$ . For each training method, test set accuracies are evaluated at each training epoch, and the best results reported. A learning rate grid search in  $\{1, 2, 5\}$  is performed for all training methods and the best result reported unless otherwise mentioned. See our experiments varying learning rate for observations on training instability beyond a learning rate of 5. We use a batch size of 100, and all methods are trained for 100 epochs unless otherwise mentioned.

**Add task experiments** The task has a sequence of iid Bernoulli inputs  $x(t)$  and desired labels  $y(t)$  constructed as:

$$y(t) = 0.5 + 0.5x(t) * \delta(t - 2) - 0.25x(t) * \delta(t - 5) \quad (53)$$

where  $*$  denotes convolution. The dataset consists of 400 labeled input sequences of length 100, split into a training dataset of 300 sequences and a test dataset of 100 sequences. Given parameters  $W_h, b_h, W_i, W_o, b_o$ , the recurrent neural network to predict  $y(t)$  is given by:

$$z_{k+1}(x) = \frac{1}{\sqrt{m}} W_h \sigma(z_k(x)) + b_h + W_i x_k \quad (54)$$

$$\hat{y}_k(x) = W_o \sigma(z_k(x)) + b_o \quad (55)$$

where  $k$  refers to the current recurrent time step,  $m$  is the size of the hidden state  $z_k(x)$ , and  $x_k$  and  $\hat{y}_k(x)$  refer to the current time input and predicted output respectively. We vary the number of hidden units in the recurrent state in a range from 8 to 4096. We train all methods with a learning rate of 0.001 and batch size 50 for 200 epochs on the mean squared error loss.

**ImageNet experiments** We train on CNN architecture with 7 convolutional layers followed by global average pooling and a fully connected layer. All convolutional layers use 3-by-3 convolutions with 512 filters. The first convolutional layer has stride 4-by-4, followed alternating convolutional layers of stride 2-by-2 and 1-by-1. All convolution layers are followed by batch normalization and a ReLU non-linearity. Networks are trained on a mean squared error loss with one-hot-encoded labels. We train on ILSVRC-12 images [28] using the following pre-processing steps: we select random crops of the original images with scales in range  $[0.08, 1.0]$  and aspect ratio in range  $[0.75, 1.34]$ ; the images are then re-scaled to 224-by-224 pixels. Next, we randomly flip images horizontally and apply a channel-wise normalization. We use a batch size of 100, and train networks using a learning rate of 5 for 200000 steps.

## F Additional tables and figures

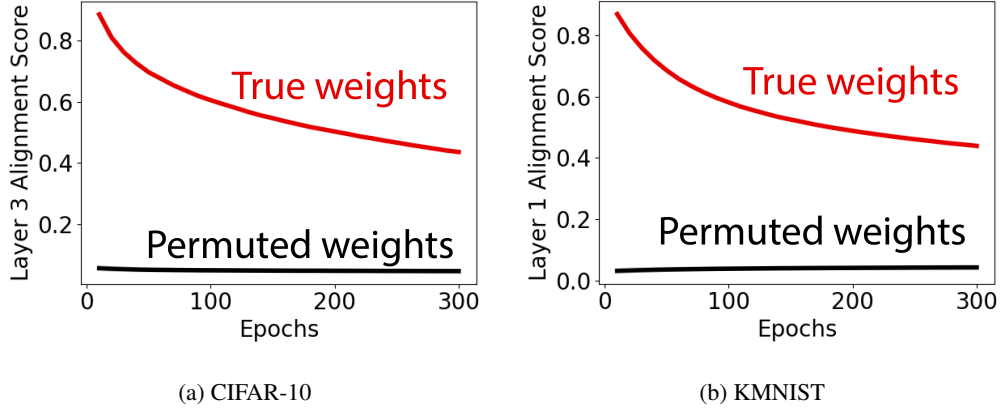


Figure 7: Alignment scores of convolutional neural networks over the course of training on the CIFAR-10 and KMNIST. As a baseline, alignment scores in networks with randomly permuted weights are also plotted. Training is conducted for 300 epochs to measure the evolution of alignment scores over a longer time-scale.

Table 1: Alignment scores of 8-layer convolutional neural networks with different layer widths trained on the CIFAR-10 dataset. The scale of the architecture is denoted  $\times n$ , where  $n$  is the number of filters in intermediate layers. Alignment scores are shown for all intermediate layers of each network after training. Non-monotonicity with layer width is due to statistical fluctuations.

Alignment	x8	x16	x32	x64	x128	x256	x512
Layer 1	0.430	0.465	0.527	0.502	0.651	0.720	0.749
Layer 2	0.490	0.433	0.409	0.409	0.656	0.658	0.760
Layer 3	0.501	0.467	0.446	0.515	0.586	0.669	0.766
Layer 4	0.372	0.297	0.350	0.371	0.497	0.703	0.767
Layer 5	0.499	0.333	0.438	0.499	0.546	0.650	0.711
Layer 6	0.301	0.363	0.329	0.321	0.419	0.500	0.603
Layer 7	0.476	0.382	0.432	0.405	0.333	0.398	0.450

Table 2: Alignment scores of 4-layer convolutional neural networks with different layer widths trained on the KMNIST dataset. The scale of the architecture is denoted  $\times n$ , where  $n$  is the number of filters in intermediate layers. Alignment scores are shown for all intermediate layers of each network after training. Non-monotonicity with layer width is due to statistical fluctuations.

Alignment	x8	x16	x32	x64	x128	x256	x512
Layer 1	0.456	0.585	0.579	0.646	0.743	0.721	0.800
Layer 2	0.137	0.179	0.210	0.299	0.381	0.482	0.656
Layer 3	0.165	0.207	0.232	0.253	0.376	0.471	0.581

Table 3: Test set accuracies of 8-layer convolutional neural networks with different layer widths on the CIFAR-10 dataset with different methods of training. The scale of the architecture is denoted  $\times n$ , where  $n$  is the number of filters in intermediate layers.

Scale	x8	x16	x32	x64	x128	x256	x512
Normal	54.8%	61.0%	64.2%	65.3%	64.2%	63.2%	62.3%
DFA [14]	28.5%	34.8%	43.0%	49.9%	54.9%	54.5%	54.1%
FA [13]	36.1%	40.3%	43.1%	46.5%	45.7%	45.6%	45.4%
Last layer	20.7%	22.5%	28.2%	31.1%	34.8%	40.2%	43.4%
<b>Align-ada</b>	<b>33.7%</b>	<b>35.7%</b>	<b>42.8%</b>	<b>49.9%</b>	<b>54.2%</b>	<b>56.6%</b>	<b>58.0%</b>
Align-zero	20.9%	22.0%	30.1%	32.6%	40.0%	47.6%	51.4%

Table 4: Test set accuracies of 4-layer convolutional neural networks with different layer widths on the KMNIST dataset with different methods of training. The scale of the architecture is denoted  $\times n$ , where  $n$  is the number of filters in intermediate layers.

Scale	x8	x16	x32	x64	x128	x256	x512
Normal	72.2%	83.4%	86.2%	87.2%	87.5%	87.4%	87.2%
DFA [14]	37.6%	49.4%	61.4%	70.7%	75.8%	77.3%	77.9%
FA [13]	52.4%	66.3%	68.6%	69.6%	72.1%	72.8%	63.5%
Last layer	25.9%	35.6%	42.2%	51.8%	58.7%	65.6%	68.2%
<b>Align-ada</b>	<b>47.5%</b>	<b>58.8%</b>	<b>70.7%</b>	<b>71.2%</b>	<b>76.1%</b>	<b>77.8%</b>	<b>78.4%</b>
Align-zero	24.5%	29.9%	31.2%	47.2%	50.3%	55.2%	61.2%

Table 5: Training and test loss for RNNs trained with normal, Align-ada, Align-zero and readout-only training on the Add task. Training losses are higher than test set losses due to the test set being an easier task: random chance loss is 9.359 on the training set and 9.312 on the test set.

Scale	x8	x16	x32	x64	x128	x256	x512	x1024	x2048	x4096
Normal, Train loss	1.168	0.553	0.495	0.527	0.474	0.440	0.429	0.408	0.412	0.429
Normal, Test loss	1.133	0.488	0.411	0.461	0.399	0.366	0.352	0.333	0.339	0.357
Align-ada, Train loss	6.652	1.944	0.782	0.772	0.786	0.535	0.474	0.455	0.450	0.466
Align-ada, Test loss	6.795	1.890	0.716	0.707	0.718	0.461	0.394	0.374	0.369	0.388
Align-zero, Train loss	5.228	2.235	1.272	0.621	0.741	0.807	0.482	0.448	0.442	0.447
Align-zero, Test loss	5.227	2.211	1.205	0.556	0.663	0.742	0.408	0.367	0.364	0.372
Readout-only, Train loss	3.008	2.798	2.011	1.872	1.674	2.655	2.202	1.881	2.042	1.647
Readout-only, Test loss	2.957	2.794	1.990	1.855	1.601	2.623	2.077	1.811	1.976	1.608